



Microspheres loaded with polysaccharide nanoparticles for pulmonary delivery: Preparation, structure and surface analysis

Sonia Al-Qadi^a, Ana Grenha^b, Carmen Remuñán-López^{a,*}

^a Department of Pharmaceutical Technology, University of Santiago de Compostela, Faculty of Pharmacy, Campus Vida, 15782-Santiago de Compostela, Spain

^b CBME-Centre for Molecular and Structural Biomedicine, IBB-Institute for Biotechnology and Bioengineering, University of Algarve, Campus de Gambelas, Faro, Portugal

ARTICLE INFO

Article history:

Received 7 January 2011

Received in revised form 21 February 2011

Accepted 11 March 2011

Available online 25 March 2011

Keywords:

Chitosan

Hyaluronic acid

Microspheres

Nanoparticles

Pulmonary administration

Spray drying

TOF-SIMS

XPS

ABSTRACT

In this work, we report the preparation of a nanoparticle-based dry powder for pulmonary administration. Hybrid chitosan/hyaluronic acid nanoparticles were produced by ionotropic gelation and characterized for their physicochemical properties, being further studied by solid nuclear magnetic resonance (NMR). Using mannitol as carrier, nanoparticles were microencapsulated by spray drying, resulting in a dry powder with appropriate aerodynamic properties for lung delivery. In order to investigate the nanoparticles distribution within the carrier matrix, several techniques were applied that permitted an in-depth analysis of the system structure and surface, such as confocal laser scanning microscopy (CLSM) and X-ray photoelectron spectroscopy (XPS) in combination with time-of-flight secondary ion mass spectroscopy (TOF-SIMS). Overall, the studies conducted revealed that nanoparticles are homogeneously distributed through mannitol microspheres, suggesting the success of the microencapsulation process. In the light of these findings, it was concluded that the developed delivery system holds great potential for lung delivery of macromolecules.

© 2011 Elsevier Ltd. All rights reserved.

1. Introduction

Presently, there is particular research interest in pulmonary delivery of drugs, specially peptides, proteins and genes, not only for local, but also for systemic effect. This is primarily due to the important advantages offered by the pulmonary route, such as the large alveolar surface available for absorption, very thin diffusion path to the blood stream, extensive vascularisation, relatively low metabolic activity compared to other routes and avoidance of gastrointestinal degradation and hepatic metabolism (Agu, Ugwoke, Armand, Kinget, & Verbeke, 2001; Courrier, Butz, & Vandamme, 2002).

In spite of this, in order to succeed in the pulmonary delivery of any therapeutic molecules, many obstacles and lung defense mechanisms, that could hinder the path of foreign substances, must be overcome, such as the effect of the airways' structure, mucociliary clearance and phagocytosis by alveolar macrophages (Courrier et al., 2002; Hastings, Folkesson, & Matthay, 2004). Thus, to evade the impact of such barriers and to assure optimal drug delivery to the desired site, it is critical to develop the appropriate drug carriers. In this respect, specific characteristics are required which provide the drug delivery system with the ability to reach the alveolar region, if a systemic effect is desired, or another specific site, if a local action is intended (Pandey & Khuller, 2005). Considering the specific anatomy of the airways, it is traditionally believed that droplets and/or particles with an aerodynamic diameter within the range of 1–3 μm will present appreciable deposition in the alveolar region, while those with a higher aerodynamic diameter will mainly deposit in the upper regions (Chrystyn, 1997). Therefore, size and density of the delivery system are the most critical parameters in obtaining adequate therapeutic effects. However, notwithstanding the referred aerodynamic requirements, nanoparticles have also been recently proposed for the same end (Bailey & Berkland, 2009; Dailey et al., 2003; Sung, Pulliam, & Edwards, 2007; Yang, Peters, & Williams, 2008) due to their ability to delay or avoid mucociliary clearance and macrophage capture (Schürch, Gehr, Im Hof, Geiser, & Green, 1990).

Abbreviations: A459, adenocarcinoma human alveolar basal epithelial cells; Calu-3, human airway epithelial cell line; CLSM, confocal laser scanning microscopy; CS, chitosan sodium hydrochloride; GlcA, glucuronic acid; GlcNAc, N-acetyl glucose amine; Glc, glucose amine; 1D-CPMAS ^{13}C , cross polarization magic angle spinning NMR; HA, hyaluronic acid; 16HBE14o, human bronchial epithelial cell line; M, mannitol microspheres; M-NPs, microencapsulated nanoparticles; Mix, physical mixture of chitosan with hyaluronic acid; NMR, nuclear magnetic resonance; NPs, nanoparticles; SEM, scanning electron microscope; TEM, transmission electron microscopy; TOF-SIMS, time-of-flight secondary ion mass spectroscopy; TPP, pentasodium tripolyphosphate; XPS, X-ray photoelectron spectroscopy.

* Corresponding author. Tel.: +34 981563100x15045; fax: +34 981547148.

E-mail address: mdelcarmen.remunan@usc.es (C. Remuñán-López).

The selection of suitable biocompatible materials (polymers, lipids, sugars) used for the preparation of lung carriers has been shown to be an essential consideration and, in this context, the polysaccharides chitosan and hyaluronan are particularly attractive polymers. Chitosan, a natural polysaccharide derived from chitin, is one of the most promising materials for transmucosal drug delivery, given its reported low toxicity, biodegradability and biocompatibility (Hirano, Seino, Akiyama, & Nonaka, 1988; Issa, Koping-Hoggard, & Artursson, 2005; Varshosaz, 2007), as well as mucoadhesivity (Agnihotri, Mallikarjuna, & Aminabhavi, 2004; Lehr, Bouwstra, Schacht, & Junginger, 1992) and enhancement of macromolecules permeation (Bernkop-Schnürch, Kast, & Guggi, 2003). Chitosan is being extensively employed in the development of micro- and nanocarriers (Grenha, Carrion-Recio, Teijeiro-Osorio, Seijo, & Remuñán-López, 2008). In fact, chitosan is known to be degraded by mammalian enzymes such as α -amylase (Muzzarelli, 1997) and lysozyme and has been demonstrated to induce low or absent toxicity in cell lines representative of the pulmonary route (16HBE140-, Calu-3 and A549) (Florea, Thanou, Junginger, & Borchard, 2005; Grenha, Grainger, et al., 2007; Lim, Forbes, Martin, & Brown, 2001).

Hyaluronic acid is a natural, linear and non-sulfated glycosaminoglycan (Bastow et al., 2008; Stern, Kogan, Jedrzejewski, & Šoltès, 2007; Theocharis et al., 2008; Volpi, Schiller, Stern, & Šoltès, 2009), which is present in human tissues and fluids, mostly in soft connective tissue. Interestingly, it can be found on the surface of alveolar epithelial cells, providing protection against tissue damage and injury in a number of respiratory diseases (Jiang, Liang, & Noble, 2007) and preventing pleural thickening in tuberculosis patients (Cantor & Turin, 2004; Zhuo, Guo, & Tang, 2003). Furthermore, it has been widely implicated in the development of drug and gene delivery systems directed to different routes of administration (Brown & Jones, 2005; Coradini et al., 2004; Gómez-Gaete et al., 2008; Hwang, Kim, Chung, & Shim, 2008; Lim, Forbes, Martin, & Brown, 2002; Peer & Margalit, 2004; Sahiner & Jia, 2008; Woo et al., 2007; Xin, Wang, & Xiang, 2010). This interesting profile of hyaluronic acid arises from its unique characteristics, such as endogeneity, biodegradability, mucoadhesivity (Avitabile et al., 2001; Morimoto, Metsugi, Katsumata, Iwanaga, & Kakemi, 2001; Mayol, Quaglia, Borzacchiello, Ambrosio, & La Rotonda, 2008; Sivadasa et al., 2008), the capacity to increase drug circulation time *in vivo* (Jiang et al., 2008; Peer & Margalit, 2004), and the ability to modify drug dissolution and absorption (Chono, Li, Conwell, & Huang, 2008). Interestingly, hyaluronic acid selectively binds to CD44 receptors expressed on lung epithelial cells and over-expressed in cancer cells, a capacity that has prompted its use for targeting purposes (Akima et al., 1996; Taetz et al., 2009). More specifically, it has been employed in drug inhalation and gene therapy, which have revealed encouraging *in vitro* and *in vivo* outcomes related to improved bioavailability and transfection (Akima et al., 1996; Hwang et al., 2008; Rouse, Whateley, Thomas, & Eccleston, 2007; Surendrakumarm, Martyn, Hodgers, Jansen, & Blair, 2003; Taetz et al., 2009). We recently proposed the preparation of chitosan/hyaluronic acid nanoparticles using a mild gelation technique (De La Fuente, Seijo, & Alonso, 2008a), which demonstrated great potential for ocular gene delivery (De La Fuente et al., 2008a; De La Fuente, Seijo, & Alonso, 2008b; De La Fuente et al., 2010). Furthermore, these nanoparticles have shown to have a potential application in the treatment of asthma, for heparin administration (Oyarzun-Ampuero, Brea, Loza, Torres, & Alonso, 2009).

It is well known that delivering nanoparticles to the lungs is impractical due to their reduced dimensions and, hence, low inertia (Sung et al., 2007; Yang et al., 2008). To address these limitations, we have recently proposed the microencapsulation of chitosan nanoparticles within a micron-sized mannitol inert carrier (Grenha, Seijo, & Remuñán-López, 2005) as an attempt to improve

the nanoparticles stability (nanoparticles are administered in solid state and, therefore, more stable than the liquid counterpart) and aerosolization pattern, by conferring adequate aerodynamic properties for proper particle deposition and drug delivery in the lungs (Azarmi et al., 2006; Freitas & Müller, 1998; Sham, Zhang, Finlay, Roa, & Löbenberg, 2004).

For a better understanding of the relation between surface properties and biological performance, it is necessary to characterize in detail the surface of the developed carrier, which entails determining the composition, structure and distribution of all components present on the surface. It has been reported, specifically for dry powders, that having information on their surface composition affords the possibility of controlling interparticulate interactions and, thus, enhancing powder dispersion during inhalation (Bosquillon et al., 2004; Bunkera, Davies, Chena, James, & Roberts, 2006; Chougule, Padhi, Jinturkar, & Misra, 2007). Thus, the investigation of surface chemistry of dry powders may be beneficial in the selection of optimal formulation and process parameters to maintain macromolecule integrity and aerosolization efficiency which definitively result in high *in vivo* outcomes.

Herein, we report the preparation of hybrid chitosan/hyaluronic acid nanoparticles and their characterization by NMR technique. These nanoparticles were microencapsulated in mannitol microspheres using the spray drying technique, rendering them adequate for pulmonary delivery. The mannitol microspheres' structure was observed by confocal laser scanning microscopy (CLSM) in order to investigate the nanoparticles' spatial distribution within mannitol microspheres following the microencapsulation process. Their surface was further analyzed by the application of two surface-sensitive analytical techniques, X-ray photoelectron spectroscopy (XPS) and static time-of-flight secondary ion mass spectrometry (TOF-SIMS), accurately characterizing their surface chemical composition and determining the presence of nanoparticles.

2. Materials and methods

2.1. Chemicals

Ultrapure chitosan in the form of hydrochloride salt (CS) (Protasan® UP Cl 113, deacetylation degree 75–90%, viscosity < 20 mPa s, molecular weight < 150 kDa) was purchased from FMC Biopolymers [Norway]; hyaluronic acid (HA) (molecular weight ~ 166 kDa) was provided by Bioiberica [Spain]; fluorescein sodium salt, phosphate buffered saline tablets (PBS) pH 7.4, pentasodium tripolyphosphate (TPP) and D-mannitol were supplied by Sigma-Aldrich [Spain] and Bodipy® 630/650-X was provided by Molecular Probes [Netherlands]. Ultrapure water [MilliQ plus, Millipore Ibérica, Spain] was used throughout. All other chemicals were reagent grade.

2.2. Preparation of chitosan/hyaluronic acid nanoparticles

Chitosan/hyaluronic acid nanoparticles were produced by a slight modification of the ionotropic gelation technique previously developed by our group (Calvo, Remuñán-López, Vila-Jato, & Alonso, 1997a, 1997b; De La Fuente et al., 2008a). Electrostatic interactions were involved in the nanoparticles formation, where the positively charged amino groups of CS interact with both negatively charged HA and TPP. Briefly, solutions of TPP and HA in ultrapure water were prepared at concentrations of 0.4–2 mg/mL (w/v) and 2–4 mg/mL (w/v), respectively, and then, equal volumes of both solutions were mixed. Thereafter, 1 mL of this mixture was added to 3 mL of CS solution whose concentration ranged from 1 to 1.25 mg/mL (w/v) and the reaction was maintained for 10 min under mild magnetic stirring, resulting in different formulations of nanoparticles as indicated in Table 1. Nanoparticles

Table 1

Process yields and physicochemical properties of chitosan/hyaluronic acid nanoparticles, prepared with different concentrations of hyaluronic acid (HA), triphosphosphate (TPP) and chitosan (CS) (mean \pm S.D., $n = 3$).

CS/HA/TPP (w/w/w)	Yield (%)	Size (nm)	Z potential (mV)
3.75/1/1	56 \pm 8	233 \pm 3	+37 \pm 2
4.3/1.1/1	44 \pm 1	239 \pm 4	+35 \pm 1
4.3/1.4/1	45 \pm 2	275 \pm 20	+34 \pm 1
5.0/1.3/1	41 \pm 4	297 \pm 23	+34 \pm 1
5.0/1.7/1	48 \pm 2	212 \pm 4	+25 \pm 1
5.0/2.5/1	56 \pm 1	254 \pm 6	+23 \pm 1
6.3/3.1/1	40 \pm 4	241 \pm 5	+20 \pm 1
7.5/3.8/1	41 \pm 3	219 \pm 7	+26 \pm 1
9.4/4.7/1	33 \pm 1	197 \pm 4	+25 \pm 1
15.0/10/1	23 \pm 9	173 \pm 1	+19 \pm 1

formed immediately and were subsequently isolated for further analysis by centrifugation on a 10 μ L glycerol layer [18,000 \times g, 30 min, 15 °C, Beckmann Avanti 30, Beckmann, USA], afterwards being re-suspended in 100 μ L of purified water after discarding the supernatants.

For confocal laser scanning microscopy (CLSM) study, CS was labeled with fluorescein following the method described by De Campos, Diebold, Carbalho, Sánchez, and Alonso (2004). Nanoparticles were also prepared on a large scale, where the final volume of nanoparticles suspension was scaled to 40 mL. In this case, centrifugation was performed for 40 min at 18,000 \times g and 15 °C.

2.3. Determination of nanoparticles production yield

The nanoparticles production yield was calculated by gravimetry. Fixed volumes of nanoparticles suspensions were centrifuged (18,000 \times g, 45 min, 15 °C), supernatants were discarded and sediments of nanoparticles were freeze-dried over 48 h (24 h set at –34 °C and gradual ascent until 20 °C), using a Labconco Freeze Dryer [Labconco, USA] ($n = 6$).

The process yield was calculated as follows:

$$\text{Process yield (\%)} = \frac{\text{nanoparticles weight}}{\text{total solids (CS + HA + TPP) weight}} \times 100$$

2.4. Physicochemical characterization of nanoparticles

The morphological appearance of nanoparticles was examined by transmission electron microscopy (TEM) [CM 12 Philips, Eindhoven, Netherlands]. The samples were previously stained with 2% phosphotungstic acid and placed on copper grids with Formvar® films for viewing.

Measurements of nanoparticles size and zeta potential were performed on freshly prepared samples, by photon correlation spectroscopy and laser Doppler anemometry, respectively, using a Zetasizer® Nano-ZS [Malvern instruments, Malvern, UK]. For particle size analysis, each sample of isolated nanoparticles was diluted to the appropriate concentration with ultrapure water. Each analysis was performed at 25 °C at a detection angle of 173 °C. For the determination of zeta potential of the electrophoretic mobility, isolated nanoparticles samples were diluted with 0.1 mM KCl and placed in an electrophoretic cell, where a potential of ± 150 mV was established. Size and zeta potential of each formulation were analyzed in triplicate ($n = 3$).

2.5. Solid NMR spectroscopy of nanoparticles

Solid-state ¹³C CP-MAS NMR spectroscopy experiments were performed at 298 K in an 11.7T Varian Inova-750 spectrometer (operating at 750 MHz proton frequency) equipped with a T3 Varian solid probe [Varian, Inc., USA]. Solid NMR samples were prepared

in 3.2 mm rotors with an effective sample capacity of 22 μ L which corresponds to approximately 30 mg of the powder sample. The spectra were processed and analyzed with MestreNova software [Mestrelab Research Inc.]. Carbon chemical shifts were assigned to the carbon methylene signal of solid adamantane at 28.92 ppm.

Four samples were analyzed: pure chitosan (CS), pure hyaluronic acid (HA), a physical mixture of equal weights of CS and HA (Mix.) and chitosan/hyaluronic acid freeze-dried nanoparticles (NPs) (CS/HA/TPP = 3.75/1/1). For each sample, a 1D-CPMAS ¹³C (cross polarization magic angle spinning) spectrum was acquired under semi-quantitative experimental conditions. The inter-scan delay was set to 3 s, the number of scans was 8000 and the MAS rate was 15 kHz. Heteronuclear decoupling during acquisition of the FID was performed with Spinal-64 with the proton field strength of 70 kHz. The cross polarization time was set to 3 ms. During cross polarization, the field strength of the proton pulse was set constant to 75 kHz and that of the ¹³C pulse was linearly ramped with a 20 kHz ramp near the matching sideband. Prior to the acquisition of the 1D-CPMAS spectra of the samples, the adamantane sample was used to calibrate the maximum ¹H–¹³C cross-polarization under the experimental conditions.

2.6. Preparation of dry powders containing chitosan/hyaluronic acid nanoparticles

Sediments of chitosan/hyaluronic acid nanoparticles (CS/HA/TPP = 3.75/1/1), obtained following centrifugation of the fresh nanoparticles suspensions, were resuspended in a mannitol aqueous solution and the resultant suspension of nanoparticles in mannitol was spray dried. Mannitol solutions were prepared with such concentrations that allowed final mannitol/nanoparticles to be obtained at ratios of 90/10, 80/20, 70/30 (w/w) and suspensions with a solid content of 3%. Dry powders were obtained in a one step process by spray drying either aqueous solutions of mannitol or suspensions of nanoparticles in mannitol using a laboratory scale drier [Büchi® Mini Spray Dryer, B-290, Switzerland]. The spray drying operating conditions were: two fluids external mixing 0.7 mm nozzle, feed rate of 2.5 mL/min and inlet temperature of 170 \pm 2 °C, resulting in outlet temperature of 111 \pm 2 °C. The air flow rate and the aspirator rate were constant at 400 NL/h and 70%, respectively. The resultant spray dried powders were collected and stored in a desiccator at room temperature until use. Preparation of microspheres for CLSM study was performed with mannitol labeled with the fluorophore Bodipy® 630/650-X, which was then mixed with the fluorescently labeled nanoparticles (described in section 2.2) and, then co-spray dried. The labeling of mannitol with Bodipy® was obtained by adding a solution of the fluorophore in dimethyl sulfoxide to a mannitol solution (0.32 μ g Bodipy®/mg mannitol), which was then kept under magnetic stirring for 1 h.

2.7. Determination of spray drying process yield

Process yield of spray drying process was determined by gravimetry establishing a comparison between the weight of resultant dry powder (microspheres) and that of the solids involved in the formulation, as follows ($n = 3$):

$$\text{Process yield (\%)} = \frac{\text{microspheres weight}}{\text{total solids (NPs + Mannitol) weight}} \times 100$$

2.8. Microspheres morphological and aerodynamic characterizations

Morphology of microspheres was viewed using a scanning electron microscope [SEM, Leo, 435VP, UK]. Dry powders were placed onto metal plates and a 200 nm thick gold palladium film was

sputter-coated on to the samples [High resolution Sputter Coater SC7640, Termo VG Scientific, UK] before viewing.

Aerodynamic diameter measurement was obtained using a TSI Aerosizer[®] LD, equipped with an Aerodisperser[®] [Amherst Process Instrument, Inc., Amherst, MA, USA], whose measuring principle is based on the measurement of particles time of flight in an air stream, according to the following equation ($n = 3$):

$$C_d \frac{\pi d^2}{4} \rho_a \frac{(V_a - V_p)}{2} = \frac{1}{6} \pi d^3 \rho_p \frac{dV_p}{dt}$$

where C_d , drag coefficient; d , particle diameter; ρ_a , density of air; V_a , velocity of air; V_p , velocity of particle; and ρ_p , density of particle.

Real density was measured using a Helium Pycnometer [Micropycnometer, Quanta Chrome, Model MPY, 2, USA]. Measurements were performed in triplicate ($n = 3$).

2.9. Structural characterization of nanoparticle-loaded microspheres using CLSM

Confocal laser scanning microscopy (CLSM) study was conducted to characterize the internal structure of nanoparticles-loaded microspheres (CS/HA/TPP = 3.75/1/1, NPs/Mannitol = 30/70 (w/w)), using a TCS-SP2 vertical microscope [Leica GmbH, Germany], which collects images using different fluorescent detectors and using, in this case, two laser lines: argon at 488 nm and helium-neon at 633 nm. Small samples of the dry powder composed of nanoparticles-loaded microspheres (fluorescein-labeled nanoparticles and Bodipy[®]-labeled mannitol) were placed on a glass slide and a drop of immersion oil was added to avoid particle displacement during viewing. Laser excitation wavelengths of 488 and 633 nm were used to scan the powder, and fluorescent emissions from fluorescein (emission $\lambda = 492$ –550 nm) and Bodipy[®] (emission $\lambda = 650$ –725 nm) were collected using separate channels. Images were acquired with a magnification of 63 \times , using an oil immersion lens (HCX PL APO lbd. BL 63 \times /1.40). The gray scale images obtained from each scan were pseudo-colored green (fluorescein) and red (Bodipy[®]), and overlapped afterwards [LCS Lite, Leica Confocal Software, Leica GmbH, Germany] to obtain a multi-coloured image.

2.10. Microspheres surface analysis using XPS and TOF-SIMS

The surface of microencapsulated nanoparticles (CS/HA/TPP = 3.75/1/1, NPs/Mannitol = 30/70 (w/w)), mannitol microspheres and chitosan/hyaluronic acid nanoparticles (CS/HA/TPP = 3.75/1/1) was analyzed by X-ray photoelectron spectroscopy (XPS) and time-of-flight secondary ion mass spectrometry (TOF-SIMS). To do so, powder samples (microencapsulated nanoparticles and mannitol microspheres) or a small drop of nanoparticles suspension were directly placed on a clean polished monocrystalline silicon wafer, used as the sample holder. In the latter case, the droplet of chitosan/hyaluronic acid nanoparticles was allowed to dry at room temperature. Mannitol microspheres and chitosan/hyaluronic acid nanoparticles were used separately as controls.

XPS analysis of the samples was performed using a Thermo Scientific K-Alpha ESCA instrument [VG Escalab 250 iXL ESCA, VG Scientific, U. K], equipped with aluminum Ka1, 2 monochromatized radiation at 1486.6 eV X-ray source. Due to the non conductor nature of samples, it was necessary to use an electron flood gun to minimize surface charging. Neutralization of the surface charge was performed using both a low energy flood gun (electrons in the range 0–14 eV) and a low energy Argon ions gun. The XPS measurements were carried out using monochromatic Al-K radiation ($\lambda\nu = 1486.6$ eV). Photoelectrons were collected from a takeoff angle of 90° relative to the sample surface. The measurement was carried

out in a Constant Analyzer Energy mode (CAE) with a 100 eV pass energy for survey spectra and 20 eV pass energy for high resolution spectra. Charge referencing was achieved by setting the lower binding energy C1s photopeak at 285.0 eV C1s hydrocarbon peak. Surface elemental composition was determined using the standard scofield photoemission cross sections.

The static time-of-flight secondary ion mass spectrometry (TOF-SIMS) analysis was performed where the mass spectra of the samples were recorded on a TOF-SIMS instrument [TOF-SIMS IV, Ion-Tof GmbH, Germany]. Samples were bombarded with a pulsed Bismuth ion beam. The secondary ions generated were extracted with a 10 kV voltage and their time of flight from the sample to the detector was measured in a reflectron mass spectrometer. Typical analysis conditions for this work were: 25 keV pulsed Bi₃⁺ beam at 45° incidence, rastered over 500 $\mu\text{m} \times 500 \mu\text{m}$. Electron flood gun charge compensation was necessary during measurements.

3. Results and discussion

3.1. Preparation and characterization of chitosan/hyaluronic acid nanoparticle

As described in the methodology section, chitosan/hyaluronic acid nanoparticles were prepared by the ionotropic gelation of the positively charged CS, mediated by the interaction with oppositely charged HA and TPP. As evidenced by TEM microphotographs displayed in Fig. 1, nanoparticles showed a spherical morphology. Table 1 depicts the physicochemical properties of the resultant nanoparticles, which exhibited a positive zeta potential (+19 to +37 mV) and small sizes in the range of 173–297 nm. The formulation CS/HA/TPP = 3.75/1/1 (w/w) was selected to conduct all subsequent experiments as it displayed the highest production yield and positive charge.

NMR is a well established technique for structural and dynamic characterization of molecules and for the study of organic reactions and processes either in solution, semi-solid or solid states. The NMR study of relatively high-molecular weight polymers, containing a number of carbon atoms, usually benefits from the use of solid NMR techniques (Mi, Sung, & Shyu, 2000). In this regard, the 1D-CPMAS ¹³C spectra of these polymers may reveal detailed information relative to their composition with semi-quantitative results (Metz, Ziliox, & Smith, 1996). ID solid-state NMR experiments were employed here to verify the cross-linking reaction between CS and HA (Fig. 2) that contributes to nanoparticles formation. More specifically, the technique can be sensitive enough to subtle changes

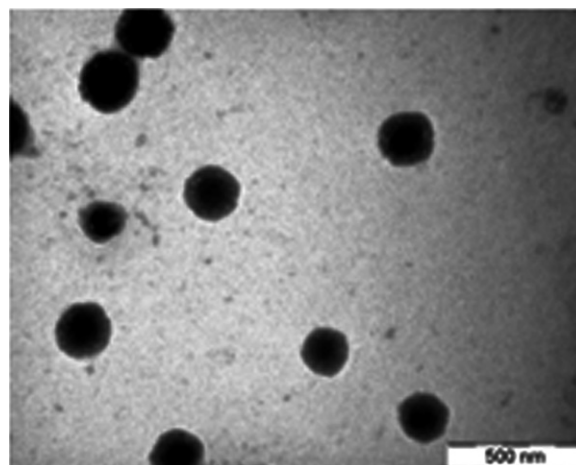


Fig. 1. TEM microphotographs of chitosan/hyaluronic acid nanoparticles (CS/HA/TPP = 3.75/1/1).

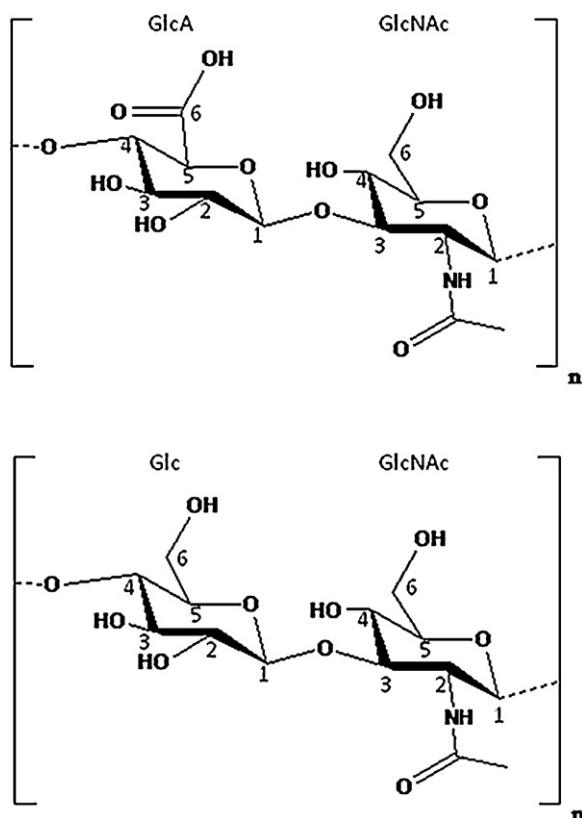


Fig. 2. A numbering scheme for hyaluronic acid (above) and chitosan (bottom) polysaccharides where GlcA, GlcNAc, and Glc refer to glucuronic acid, N-acetyl glucose amine and glucose amine, respectively.

in the electronic environments of the carbon atoms of CS and HA when they are ionically cross-linked to generate the nanoparticles. To perform this study, four samples were analyzed: nanoparticles (CS/HA/TPP = 3.75/1/1 (w/w)), pure CS and HA polymers and the physical mixture of CS and HA (Mix). The corresponding 1D-CPMAS ^{13}C spectra are displayed in Fig. 3, each of which contains three broad signals that overlap in the band between 43 and 110 ppm, which is the typical region of the sugar ring carbons from C1 to C6. The signals in this band can be assigned as follows: (i) region 95–110 ppm corresponds to the C1 anomeric carbons of the polymer, (ii) region 70–95 ppm corresponds to the carbons C2–C5 of the polymer and (iii) region 43–70 ppm corresponds to the C6 methylene carbons of the polymer. The four spectra also show the characteristic peak at ca. 174 ppm corresponding to the carboxylate and/or carbonyl acetamide carbons, as well as the carbon peak at ca. 24 ppm corresponding to the methyl group of the acetamide group. According to these observations, all spectra elucidate the essential pattern of signals related to polysaccharide structure, but are different in the relative intensities, as depicted in Table 2. Inter-

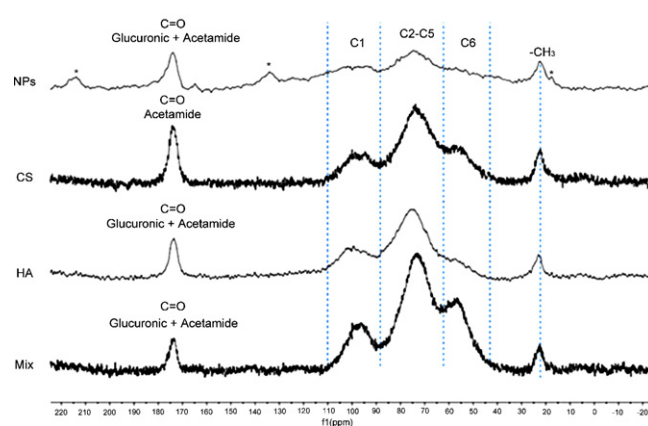


Fig. 3. Solid-state ^{13}C -NMR spectra of chitosan/hyaluronic acid nanoparticles (NPs) (CS/HA/TPP = 3.75/1/1), chitosan (CS), hyaluronic acid (HA), and the physical mixture of CS with HA (Mix) (CS/HA = 3.75/1). The signal assignment is indicated. In the spectrum of NPs, some signals that are not present in the other samples are labeled with an asterisk and discussed in the text.

estingly, the integration of the signals, in Table 2, is consistent with the structures of these polymers.

According to Fig. 3, there is a remarkable difference between the spectrum of nanoparticles and the other spectra, as signals in the first are considerably broader and extend over a larger region than the corresponding signals in the other spectra. Moreover, some new signals appear in the spectrum of nanoparticles, which are indicated with asterisk. The new carbon signals, resonating at ca. 135 and 205 ppm, correspond to spinning sidebands from the CO carbonyl group at ca. 175 ppm. Their presence is indicative of enhanced chemical shift anisotropy of the CO group. There is also an additional signal at ca. 19 ppm that is presumably due to a methyl group of acetamide. These changes occurring to the acetamide group of CS could possibly result from re-organization due to ionic interactions between the randomly cross-linked rings of CS and HA, with effects utterly leading to a higher heterogeneity and broadening of signals in the NMR spectrum. Similar observations were described by others for solid NMR spectra of gel based systems (Saiò, Tuzi, & Naito, 1998). We can conclude, thereby, that the aforementioned changes detected in the 1D-CPMAS ^{13}C spectra could confirm the hypothesis of the mechanism of nanoparticles formation, which involves cross-linking via electrostatic and hydrophobic interactions between the CS and HA in addition to that contributed by the TPP cross-linker through the gelation process.

3.2. Microspheres preparation and characterization

Nanoparticles were co-spray dried with mannitol in a one-step spray drying process with yields around 65–70%. As stated in the introduction, the microencapsulation step envisages the improvement of nanoparticles aerosolization pattern and lung deposition, which are mainly driven by the aerodynamic parameters of inhaled

Table 2

Chemical shifts (ppm) and signal integrations obtained from the ^{13}C 1D-CPMAS spectra of the samples studied: pure chitosan (CS), pure hyaluronic acid (HA), physical mixture of both polymers (Mix), and chitosan/hyaluronic acid nanoparticles (NPs) (CS/HA/TPP = 3.75/1/1). The relative area of the ^{13}C NMR signal is indicated between parentheses.

Simple	C1 to C6 (sugar) ^a	CO (acetamide) ^b	CO (glucuronic) ^b	CH ₃ (acetamide) ^c	CO ^d
CS	43–110 (27.3)	174.2 (1.0)	–	22.8 (0.8)	–
HA	43–110 (7.26)	–	173.6 (1.0)	22.6 (0.39)	–
Mix	43–110 (7.75)	–	173.9 (1.0)	22.6 (0.67)	–
NPs	43–110 (7.75)	–	174.2 (1.0)	22.6 (0.98)	214.0 (0.31)

^a Integral from 43 to 110 ppm.

^b Integral from 163 to 185 ppm.

^c Integral from 12 to 34 ppm.

^d Integral from 205 to 222 ppm.

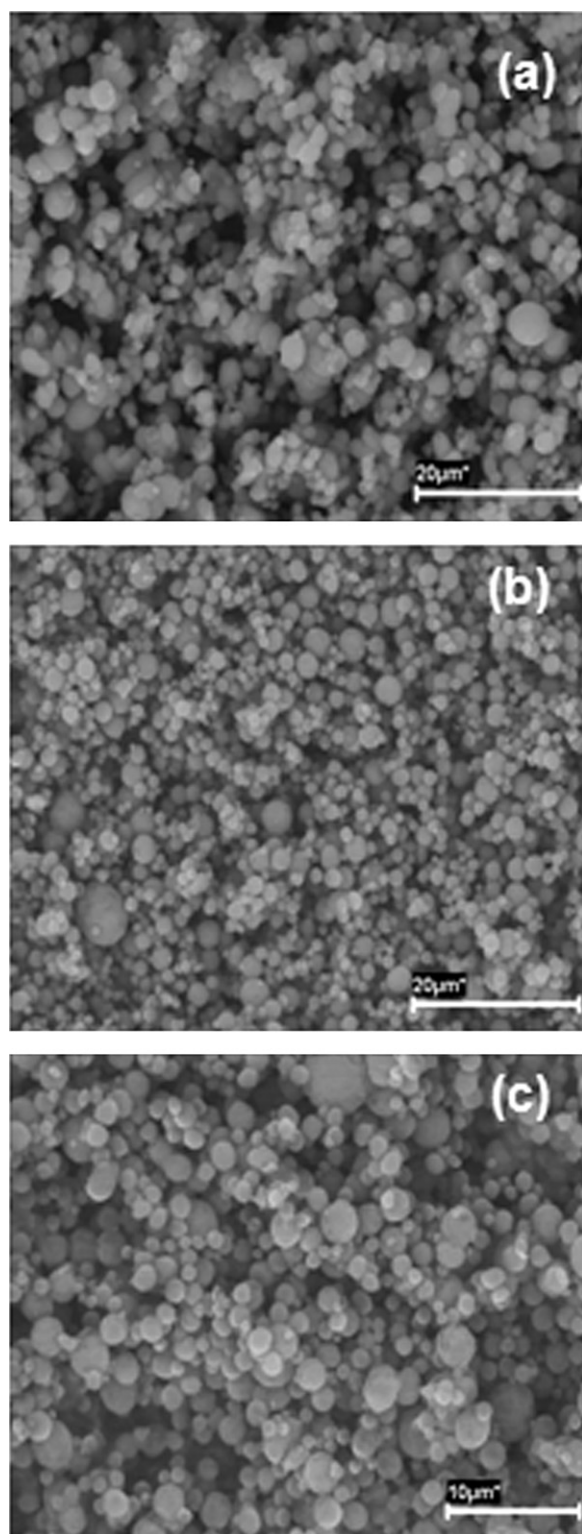


Fig. 4. SEM microphotographs of microencapsulated chitosan/hyaluronic acid nanoparticles (CS/HA/TPP=3.75/1/1) at different mannitol/nanoparticles theoretical ratios (w/w): (a) 90/10, (b) 80/20, (c) 70/30.

particles (e.g. size, density) (Larhrib, Martin, Prime, & Marriott, 2003; Minne, Boireau, Horta, & Vanbever, 2008; Vanbever et al., 1999). The resultant microencapsulated nanoparticles were viewed by SEM (Fig. 4), evidencing spherical morphology and demonstrating less tendency to aggregate as the nanoparticles load increased with respect to mannitol. Microspheres exhibited a real density

of 1.45 g/cm^3 and an aerodynamic diameter of $2.6 \mu\text{m}$ (Table 3), which are suitable characteristics to achieve deep lung deposition (Bosquillon, Lombry, Pr  at, & Vanbever, 2001; Mustante et al., 2002).

The application of sensitive techniques to characterize the structure of dry powders provides important information that helps to elucidate the behavior of these drug delivery systems in subsequent studies, both *in vitro* and *in vivo*. CLSM has been used to this end, since it allows us to acquire high resolution optical sections of x–y scans along the z-axis, which are then reconstructed into 3-D multicoloured views, enabling a complete visualization of the dry powder external and internal structure, as well as the spatial arrangement of the components (Lamprecht, Sch  fer, & Lehr, 2000). In our work, the acquisition of fluorescent images by CLSM enabled us to precisely detect the nanoparticles location within the microspheres. This could not be attained by SEM, which only provides information on the particles surface structure, rather than its internal structure. Fig. 5(a–c) displays the images of microsphere encapsulating chitosan/hyaluronic acid nanoparticles. An outer shell composed of mannitol (red channel) and an even distribution of chitosan/hyaluronic acid nanoparticles throughout the microsphere matrix can be observed. The presence of a mannitol outer shell is confirmed by Fig. 5(d), which further evidences microspheres spherical shape as previously observed by SEM. The homogeneous nanoparticles distribution within the mannitol microspheres without detecting any punctuate green signals of aggregated particles in the microspheres matrix may lead to the assumption that mannitol is almost entirely located at the particles' surface. This was also verified by the optical cross-sections of the confocal images (not shown) which suggest that the microsphere matrix is almost occupied by the fluorescent nanoparticles. It has been shown that sugar stabilizers, like mannitol, tend to preferentially adsorb at the air/liquid interface during the drying process (Arakawa & Timasheff, 1982; Wang, Chua, & Wang, 2004). Therefore, we may hypothesize that non-specific interactions occurred between the mannitol and the hydrophobic fluorophore (Bodiby  ), displacing the positively charged nanoparticles inwards. It is noteworthy that these findings are similar to those reported in previous studies for microparticles designed for inhalation therapy (Ely, Roa, & Finlay, 2007).

XPS and TOF-SIMS represent a complementary approach as non destructive and surface-sensitive analytic techniques. However, the particular interest of their application in the study of drug delivery systems arises from the capability of these techniques to provide quantitative and qualitative information of surface composition (De Vries, 1998), which provides valuable information for the interpretation of kinetic and dynamic behavior, such as drug dissolution, stability, distribution and release (Chesko et al., 2008; Dahlberg, Millqvist-Fureby, & Schuleit, 2008). Additionally, using these tools, the encapsulation efficiency of microencapsulated drugs (Morales, Ruiz, Oliva, Oliva, & Gallardo, 2007; Xie, Marijnissen, & Wang, 2006) or nanoparticles (Grenha, Seijo, Serra, & Remu    n-L  pez, 2007) can also be assessed. This latter approach was our goal in the present study. Considering the fact that microspheres have a lot of surface contact due to their powdery nature, the adsorption of atmospheric natural contaminants such as nitrogen (N), is highly probable, therefore sample surfaces were sputter cleaned using a soft argon ion beam ($\text{Ar}^+/1 \text{ kV}/60 \text{ s}$, $2 \text{ mm} \times 1 \text{ mm}$). The signals of the contaminating N in the powder samples almost disappeared (preliminary data not shown), indicating that it was weakly bound (adsorbed) and, thus, easily removed.

As displayed in Table 4, however very weak N signals were detected in these samples (values below 0.1 at%), which could be explained on the basis that the ionic barrel is 45° to the surface, generating areas of shadow where the argon ions cannot reach. By

Table 3Aerodynamic properties of dry powders prepared with different mannitol/nanoparticles weight ratios and solids contents (CS/HA/TPP = 3.75/1/1, mean \pm S.D., $n = 3$).

Mannitol/nanoparticles ratio	Solids content ^a (%)	Feret's diameter ^b (μm)	Real density (g/cm^3)	Aerodynamic diameter (μm)
70/30	3.0	2.3 ± 0.7	1.45 ± 0.06	2.57 ± 0.08
80/20	2.8	2.7 ± 1.3	1.45 ± 0.12	ND
90/10	3.0	2.2 ± 0.4	1.45 ± 0.17	ND

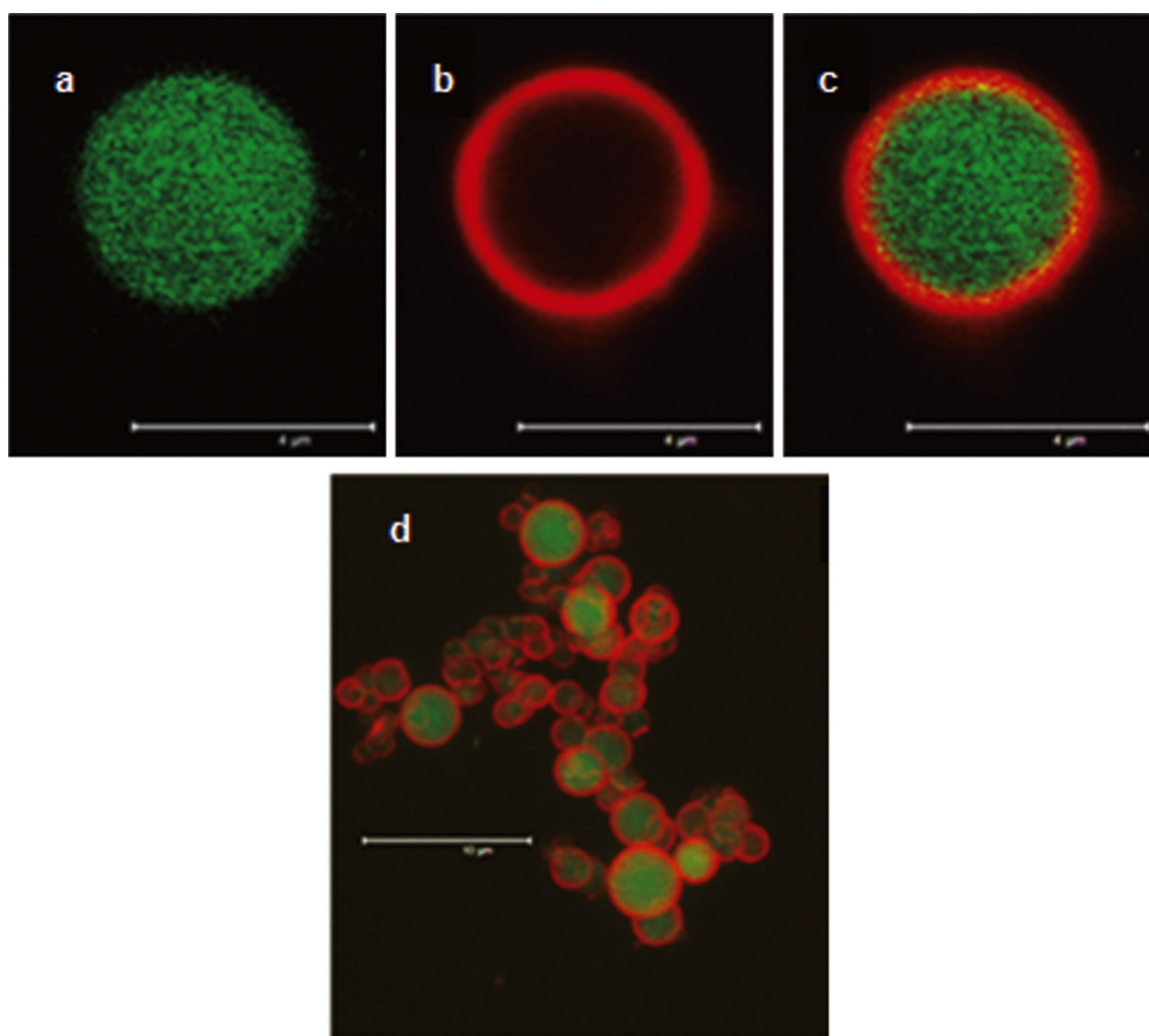
^a Solids content represents the total solids concentration (%) of the spraying suspensions.^b Feret's diameters are determined by optical microscopy.

Fig. 5. Confocal microscopy images of a mannitol microsphere loaded with chitosan/hyaluronic acid nanoparticles (CS/HA/TPP = 3.75/1/1, mannitol/nanoparticles = 30/70 (w/w): (a) a green channel representing the fluorescently labeled nanoparticles, (b) a red channel representing mannitol labeled with Bodipy[®], (c) channels overlapping; and (d) a section of mannitol microspheres containing the nanoparticles with both overlapping channels. The scale bars in panels (a–c) amounts to 4 μm and that in panel (d) amounts to 10 μm . (For interpretation of the references to color in this figure legend, the reader is referred to the web version of the article.)

Table 4

Surface elemental composition (atomic %), determined by XPS, of chitosan/hyaluronic acid nanoparticles (CS/HA NPs), mannitol microspheres (M) and microencapsulated nanoparticles (M-NPs) (CS/HA/TPP = 3.75/1/1, mannitol/nanoparticles = 70/30).

Element (%)	CS/HA NPs	M	M-NPs
C	53.2	52.5	43.0
O	33.5	45.6	38.5
N	5.2	0.10	0.10
Na	1.4	0	0
P	4.6	0	0
Si	1.4	0	12.5
S	0.7	1.7	5.9
Ratio C/O	1.6	1.15	1.12

C, carbon; O, oxygen; N, nitrogen; Na, sodium; P, phosphorus; Si, silicon; S, sulphur.

contrast, the N signal in the chitosan/hyaluronic acid nanoparticles spectrum persisted after the sputter cycle with a relatively high value, suggesting that it is chemically bonded and which could be ascribed to CS. Moreover and as expected, both Na and P, ascribed to TPP in the nanoparticles, were detected solely on the surface of chitosan/hyaluronic acid nanoparticles; whereas were absent on the surface of either mannitol microspheres or microencapsulated nanoparticles. Taking into account the detection limit of XPS (all elements except H: ~ 0.01 monolayer, or $\sim 0.1\%$ bulk), this finding indicates the absence of TPP on the powder surfaces. Our assumption of efficient nanoparticles microencapsulation can be further reinforced by the C/O ratio, which is similar for mannitol microspheres and the microencapsulated nanoparticles (1.15 and 1.12, respectively). Interestingly, this ratio is different from that

Table 5

The relative peak area (%) of each carbon environment for chitosan/hyaluronic acid nanoparticles (CS/HA NPs), mannitol microspheres (M) and microencapsulated nanoparticles (M-NPs) (CS/HA/TPP = 3.75/1/1, mannitol/nanoparticles = 70/30).

Sample	C–C/C–H 285 (eV)	C–O 286.8 (eV)	C=O 288.4 (eV)	O–C=O 289.5 (eV)
CS/HA NPs	36.0	45.7	14.2	4.1
M	29.3	61.6	9.1	0
M-NPs	39.0	56.1	4.9	0

of chitosan/hyaluronic acid nanoparticles (1.6), suggesting that the surfaces of both mannitol microspheres and the microencapsulated nanoparticles are similar in terms of the atomic composition and concentrations of C and O. Additionally, the higher C/O ratio for the chitosan/hyaluronic acid nanoparticles implies lower surface concentration of O, which is due to the contribution of other elements detected on the surface. It is worth while to notice here that a signal for silicon was identified in some spectra which could be originated from the silicon wafer used as a sample support during the analysis (Grenha, Seijo, et al., 2007).

This result was also confirmed by deconvolution analysis of the spectra where the high resolution spectra of carbon (C1s) signals, showing an envelope, were curve fitted using the Gaussian distribution into a series of peaks corresponding to different functional groups. We have assigned as reference the peak at the lowest binding energy (285.0 eV) to carbon atoms linked to carbon and hydrogen atoms. Table 5 summarizes the relative peak area (%) and relative intensities of (C–C, 285 eV), (C–O, 286.8 eV) and (C=O, 288.37 eV) are nearly similar in mannitol microspheres and microencapsulated nanoparticles. More importantly, the peak of (O–C=O, 289.54 eV), unique for CS, was detected in the spectrum of chitosan/hyaluronic acid nanoparticles but not in the other two samples. The analysis of deconvoluted C1s high resolution spectra

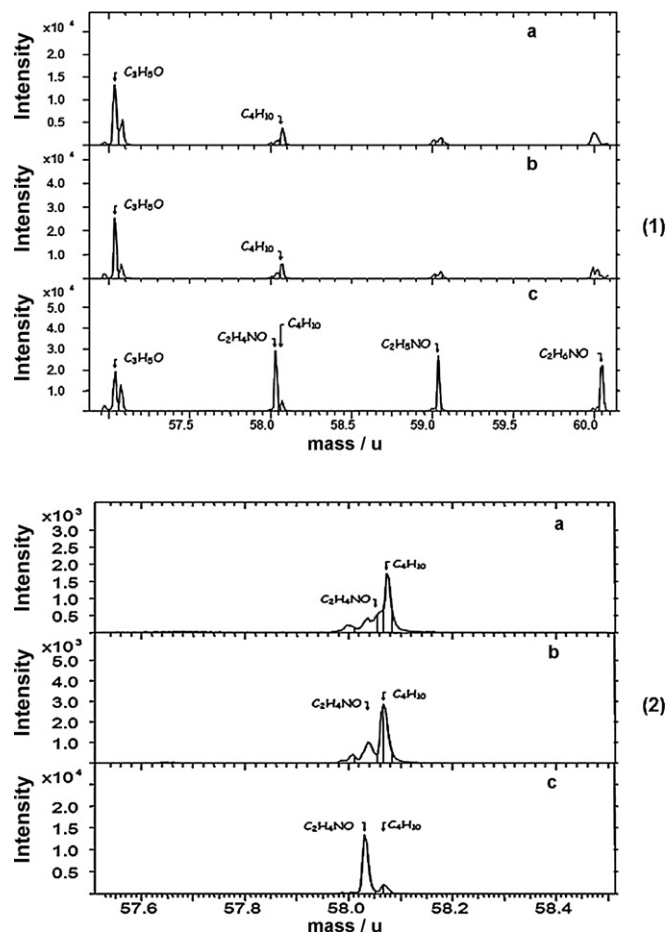


Fig. 7. Mass spectra obtained by TOF-SIMS, showing (1): N and O containing fragments in (a) mannitol microspheres, (b) microencapsulated nanoparticles (CS/HA/TPP = 3.75/1/1, NPs/Mannitol = 30/70 (w/w)), (c) chitosan/hyaluronic acid nanoparticles (CS/HA/TPP = 3.75/1/1); and (2): the fragment C_2H_4NO at $m/z = 58$ in the same samples.

re-affirms that chitosan/hyaluronic acid nanoparticles are entirely encapsulated in mannitol microspheres.

TOF-SIMS analysis was conducted under non-destructive energetic conditions and under the static limit (10^{12} ions/cm³). In the mass spectra, positive ions were detected. According to the spectra displayed in Fig. 6, the nanoparticles spectrum differs from those of both microsphere samples in the existence of some molecular fragments [$m/z = 232(C_{16}H_{24}O)$, $205(C_{15}H_{16}O)$, $200(C_{10}H_{16}O_4)$] in addition to the main and most representative ions of mannitol observed at $m/z = 183$ (the molecular ion + H) and the two times molecular ion + H observed at $m/z = 365$. At the same time, many identified molecular fragments of nanoparticles, not observed in the spectra of microspheres and located at $m/z = 189(C_7H_{13}O_4Si)$, $202(C_{12}H_{10}O_3)$, $215(C_{11}H_{12}O_3Na)$, $239(C_{15}H_{11}O_3)$ and $226(C_{18}H_{10})$, could result basically from the fragmentation of both CS and HA. Furthermore, other intensive signals for fragments containing N and O are clearly observed in the nanoparticles but not in mannitol microspheres and microencapsulated nanoparticles, located at $m/z = 60(C_2H_6NO)$, $59(C_2H_5NO)$, $58(C_2H_4NO)$ and which could arise from the fragmentation of CS (Fig. 7-1). The N-containing fragment (C_2H_4NO , $m/z = 58$), identified as intensive in the nanoparticles sample, was detected however in both microsphere samples but in one order of magnitude lower, which is likely due to the atmospheric exposure as mentioned previously (Fig. 7-2). Importantly, the PO_3 fragment ($m/z = 79$), attributed to TPP, is intensive and clearly observed in the

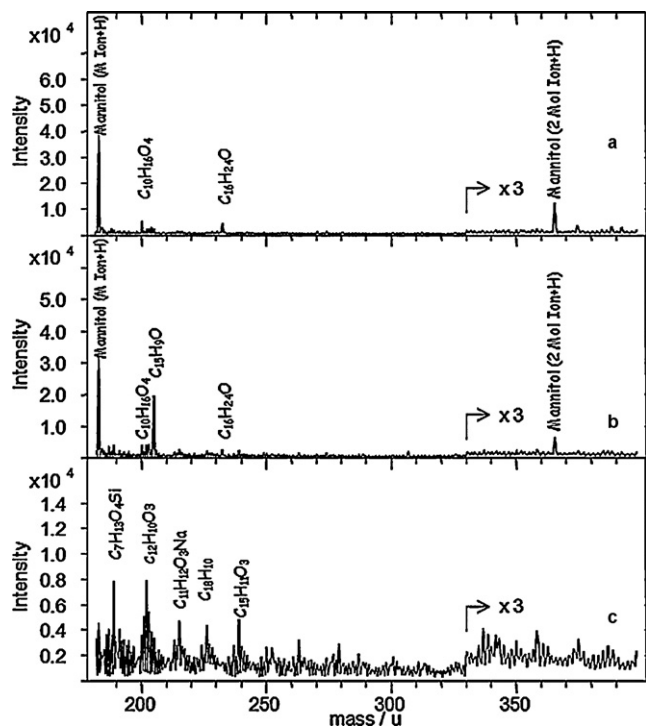


Fig. 6. Mass spectra obtained by TOF-SIMS, showing the region of molecular ion + H⁺ of mannitol for (a) mannitol microspheres, (b) microencapsulated nanoparticles (CS/HA/TPP = 3.75/1/1, mannitol/nanoparticles = 70/30 (w/w)) and (c) chitosan/hyaluronic acid nanoparticles (CS/HA/TPP = 3.75/1/1).

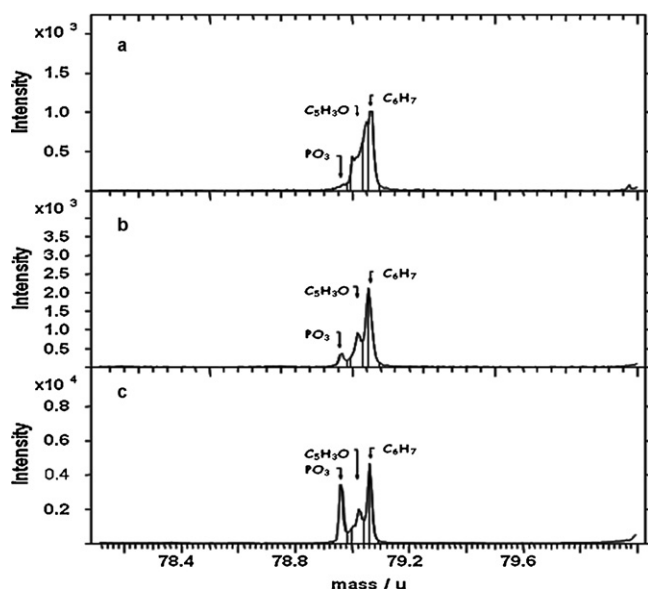


Fig. 8. Mass spectra obtained by TOF-SIMS, showing the region of phosphate fragments for the samples: (a) mannitol microspheres, (b) microencapsulated nanoparticles (CS/HA/TPP = 3.75/1/1, mannitol/nanoparticles = 70/30 (w/w)), (c) chitosan/hyaluronic acid nanoparticles (CS/HA/TPP = 3.75/1/1).

nanoparticles sample whereas it is not detected in that of mannitol microspheres and its intensity in microencapsulated nanoparticles is at least one order of magnitude lower than that of nanoparticles sample (Fig. 8).

According to our observations from these spectra, the samples of mannitol microspheres and the microencapsulated nanoparticles, if not identical, are very similar (intensity of the identified fragments and also the distribution of the intensity between ions). These outcomes demonstrate that chitosan/hyaluronic acid are efficiently encapsulated within the mannitol carrier, especially if we refer to the fact that the TOF-SIMS technique is qualified with the highest surface sensitivity for surface analysis (detection limit range of ppm–ppb, orders of magnitude better than XPS) and the resolution depth of 1–3 monolayers.

4. Conclusion

Chitosan/hyaluronic acid nanoparticles were prepared, characterized and microencapsulated in mannitol microspheres, resulting in a dry powder that shows adequate aerodynamic properties for deep pulmonary deposition. Following the encapsulation process, structural analysis of the dry powder was provided by CLSM, which elucidated that the nanoparticles were homogeneously distributed within the mannitol microsphere. The evidence that nanoparticles were completely encapsulated within the carrier by means of the spray drying process, was achieved by application of the sensitive surface analysis techniques, XPS and TOF-SIMS. These outcomes confirm the success of nanoparticles microencapsulation by spray drying. We expect, thereby, that the microencapsulated nanoparticles hold promise for pulmonary delivery of macromolecules such as proteins and nucleic acids, as these nanoparticles have demonstrated great potential in gene transfection in ocular cell lines (De La Fuente et al., 2008b). Therefore, further work is required to investigate the delivery potential of these developed carriers, in the form of dry powders in pulmonary cell lines.

Acknowledgments

The authors gratefully acknowledge support from the Spanish Government (PN de I+D 2008–2011, ISCIII-Subdirección General

de Evaluación y Fomento de la Investigación, Acción Estratégica de Salud, Project FIS, PS09/00816), XUNTA de Galicia (Dirección Xeral de I+D+I, Project PGIDIT, 09CSA022203PR, NANOPULMOGENIC; Project Competitive Reference Groups, 2010/18-FEDER), Portuguese Foundation for Science and Technology (Project PTDC/SAU-FCF/100291/2008) and IBB/CBME, LA. MAEC-AECID fellowship of the Spanish Agency of International Cooperation to S. Al-Qadi is gratefully recognized. Valuable discussions with M. M. Pastor (NMR Service, University Santiago de Compostela) and C. Serra (Centre for Scientific and Technological Support to Research, University of Vigo, E-36310, Vigo, Spain) are highly appreciated.

References

- Agnihotri, S. A., Mallikarjuna, N. N., & Aminabhavi, T. M. (2004). Recent advances on chitosan-based micro- and nanoparticles in drug delivery. *Journal of Controlled Release*, 100, 5–28.
- Agu, R. U., Ugwoke, M. I., Armand, M., Kinget, R., & Verbeke, N. (2001). The lung as a route for systemic delivery of therapeutic proteins and peptides. *Respiratory Research*, 2, 198–209.
- Akima, K., Ito, H., Iwata, Y., Matsuo, K., Watari, N., Yanagi, M., et al. (1996). Evaluation of antitumor activities of hyaluronate binding antitumor drugs: Synthesis, characterization and antitumor activity. *Journal of Drug Targeting*, 4, 1–8.
- Arakawa, T., & Timasheff, S. N. (1982). Stabilization of protein structure by sugars. *Biochemistry*, 21, 6536–6544.
- Avitabile, T., Marano, F., Castiglione, F., Bucolo, C., Cro, M., Ambrosio, L., et al. (2001). Biocompatibility and biodegradation of intravitreal hyaluronan implants in rabbits. *Biomaterials*, 22, 195–200.
- Azarmi, S., Tao, X., Chen, H., Wang, Z., Finlay, W. H., Löbenberg, R., et al. (2006). Formulation and cytotoxicity of doxorubicin nanoparticles carried by dry powder aerosol particles. *International Journal of Pharmaceutics*, 319, 155–161.
- Bailey, M. M., & Berkland, C. J. (2009). Nanoparticle formulations in pulmonary drug delivery. *Medicinal Research Reviews*, 29, 196–212.
- Bastow, E. R., Byers, S., Goluba, S. B., Clarkinc, C. E., Pittsillides, A. A., & Fosang, A. J. (2008). Hyaluronan synthesis and degradation in cartilage and bone. *Cellular and Molecular Life Sciences*, 65, 395–413.
- Bernkop-Schnürch, A., Kast, C. E., & Guggi, D. (2003). Permeation enhancing polymers in oral delivery of hydrophilic macromolecules: Thiomers/GSH systems. *Journal of Controlled Release*, 93, 95–103.
- Bosquillon, C., Lombry, C., Préat, V., & Vanbever, R. (2001). Influence of formulation excipients and physical characteristics of inhalation dry powders on their aerosolization performance. *Journal of Controlled Release*, 70, 329–339.
- Bosquillon, C., Rouxhet, P. G., Ahimou, F., Simon, D., Culot, C., Préat, V., et al. (2004). Aerosolization properties, surface composition and physical state of spray dried protein powders. *Journal of Controlled Release*, 99, 357–367.
- Brown, M. B., & Jones, S. A. (2005). Hyaluronic acid: A unique topical vehicle for the localized delivery of drugs to the skin. *Journal of the European Academy of Dermatology and Venereology*, 19, 308–318.
- Bunkera, M. J., Daviesa, M. C., Chena, X., James, M. B., & Roberts, J. C. (2006). Single particle friction on blister packaging materials used in dry powder inhalers. *European Journal of Pharmaceutical Sciences*, 29, 405–413.
- Calvo, P., Remuñán-López, C., Vila-Jato, J. L., & Alonso, M. J. (1997a). Chitosan and chitosan/ethylene oxide-propylene oxide block copolymer nanoparticles as novel carriers for proteins and vaccines. *Pharmaceutical Research*, 14, 1431–1436.
- Calvo, P., Remuñán-López, C., Vila-Jato, J. L., & Alonso, M. J. (1997b). Novel hydrophilic chitosan-polyethylene oxide nanoparticles as protein carriers. *Journal of Applied Polymer Science*, 63, 125–132.
- Cantor, J. O., & Turin, G. M. (2004). Can exogenously administered hyaluronan improve respiratory function in patients with pulmonary emphysema? *Chest*, 125, 288–292.
- Chesko, J., Kazzaz, J., Ugozzoli, M., Singh, M., O'hagan, D., Madden, C., et al. (2008). Characterization of antigens adsorbed to anionic PLG microparticles by XPS and TOF-SIMS. *Journal of Pharmaceutical Sciences*, 97, 1443–1453.
- Chono, S., Li, S.-D., Conwell, C. C., & Huang, L. (2008). An efficient and low immunostimulatory nanoparticle formulation for systemic siRNA delivery to the tumor. *Journal of Controlled Release*, 131, 64–69.
- Chougule, M. B., Padhi, B. K., Jinturkar, K. A., & Misra, A. (2007). Development of dry powder inhalers. *Recent Patents on Drug Delivery and Formulation*, 1, 11–21.
- Chrystyn, H. (1997). Is total particle dose more important than particle distribution? *Respiratory Medicine*, (Suppl. A), 17–19.
- Coradini, D., Pellizzaro, C., Abolafio, G., Bosco, M., Scarlata, I., Cantoni, S., et al. (2004). Hyaluronic-acid butyric esters as promising antineoplastic agents in human lung carcinoma: A preclinical study. *Investigational New Drugs*, 22, 207–217.
- Courrier, H. M., Butz, N., & Vandamme, T. F. (2002). Pulmonary drug delivery systems: Recent developments and prospects. *Critical Reviews in Therapeutic Drug Carrier Systems*, 19, 425–498.
- Dahlberg, C., Millqvist-Fureby, A., & Schuleit, M. (2008). Surface composition and contact angle relationships for differently prepared solid dispersions. *European Journal of Pharmaceutics and Biopharmaceutics*, 70, 478–485.
- Dailey, L. A., Kleemann, E., Wittmar, M., Gessler, T., Schmehl, T., Roberts, C., et al. (2003). Surfactant-free, biodegradable nanoparticles for aerosol therapy based

- on the branched polyesters, DEAPA-PVAL-g-PLGA. *Pharmaceutical Research*, 20, 2011–2020.
- De Campos, A. M., Diebold, Y., Carbalho, E. L. S., Sánchez, A., & Alonso, M. J. (2004). Chitosan nanoparticles as new ocular drug delivery systems: In vitro stability, in vivo fate and cellular toxicity. *Pharmaceutical Research*, 21, 803–810.
- De La Fuente, M., Seijo, B., & Alonso, M. J. (2008a). Novel hyaluronan-based nanocarriers for transmucosal delivery of macromolecules. *Macromolecular Bioscience*, 8, 441–450.
- De La Fuente, M., Seijo, B., & Alonso, M. J. (2008b). Novel hyaluronic acid-chitosan nanoparticles for ocular gene therapy. *Investigative Ophthalmology and Visual Science*, 49, 2016–2024.
- De La Fuente, M., Raviña, M., Paolicelli, P., Sanchez, A., Seijo, B., & Alonso, M. J. (2010). Chitosan-based nanocarriers: A delivery platform for ocular therapeutics. *Advanced Drug Delivery Reviews*, 62, 100–117.
- De Vries, E. (1998). Surface characterization methods-XPS, TOF-SIMS, and SAM A complimentary ensemble of tools. *Journal of Materials Engineering and Performance*, 7, 303–311.
- Ely, L., Roa, W., & Finlay, W. H. R. (2007). Löbnerberg, Effervescent dry powder for respiratory drug delivery. *European Journal of Pharmaceutics and Biopharmaceutics*, 65, 346–353.
- Florea, B. I., Thanou, M., Junginger, H. E., & Borchard, G. (2005). Enhancement of bronchial octreotide absorption by chitosan and N-trimethylchitosan shows linear in vitro/in vivo correlation. *Journal of Controlled Release*, 110, 353–361.
- Freitas, C., & Müller, R. H. (1998). Spray drying of solid lipid nanoparticles (SLNTM). *European Journal of Pharmaceutics and Biopharmaceutics*, 46, 145–151.
- Gómez-Gaete, G., Tsapis, N., Silva, L., Bourgaux, C., Besnard, M., Bocho, A., et al. (2008). Supramolecular organization and release properties of phospholipid hyaluronan microparticles encapsulating dexamethasone. *European Journal of Pharmaceutics and Biopharmaceutics*, 70, 116–126.
- Grenha, A., Seijo, B., & Remuñán-López, C. (2005). Microencapsulated chitosan nanoparticles for lung protein delivery. *European Journal of Pharmaceutical Sciences*, 25, 427–437.
- Grenha, A., Grainger, C. I., Dailey, L. A., Seijo, B., Martin, G. P., Remuñán-López, C., et al. (2007). Chitosan nanoparticles are compatible with respiratory epithelial cells in vitro. *European Journal of Pharmaceutical Sciences*, 31, 73–84.
- Grenha, A., Seijo, B., Serra, C., & Remuñán-López, C. (2007). Chitosan nanoparticle-loaded mannitol microspheres: Structure and surface characterization. *Biomacromolecules*, 8, 2072–2079.
- Grenha, A., Carrion-Recio, D., Teijeiro-Osorio, D., Seijo, B., & Remuñán-López, C. (2008). Nano- and microparticulate carriers for pulmonary drug delivery. In M. N. V. Kumar (Ed.), *Handbook of particulate drug delivery (applications)* (pp. 165–192). Valencia, CA: American Scientific Publishers.
- Hastings, R. H., Folkesson, H. G., & Matthay, M. A. (2004). Mechanism of alveolar protein clearance in the intact lung. *American Journal of Physiology – Lung Cellular and Molecular Physiology*, 286, 679–689.
- Hirano, S., Seino, H., Akiyama, Y., & Nonaka, I. (1988). Biocompatibility of chitosan by oral and intravenous administrations. *Polymer Materials and Science Engineering*, 59, 897–901.
- Hwang, S. M., Kim, D., Chung, S. J., & Shim, C. K. (2008). Delivery of ofloxacin to the lung and alveolar macrophages via hyaluronan microspheres for the treatment of tuberculosis. *Journal of Controlled Release*, 129, 100–106.
- Issa, M., Koping-Hoggard, M., & Artursson, P. (2005). Chitosan and the mucosal delivery of biotechnology drugs. *Drug Discovery Today: Technologies*, 2, 1–6.
- Jiang, D., Liang, J., & Noble, P. W. (2007). Hyaluronan in tissue injury and repair. *Annual Review of Cell and Developmental Biology*, 23, 435–461.
- Jiang, G., Park, K., Kim, J., Kim, K. S., Oh, E. J., Kang, H., et al. (2008). Hyaluronic acid-polyethyleneimine conjugate for target specific hyaluronin intracellular delivery of siRNA. *Biopolymers*, 89, 635–642.
- Lamprecht, A., Schäfer, U. F., & Lehr, C.-M. (2000). Structural analysis of microparticles by confocal laser scanning microscopy. *AAPS PharmSciTech*, 1, 10–19.
- Larhrib, H., Martin, G. P., Prime, D., & Marriott, C. (2003). Characterisation and deposition studies of engineered lactose crystals with potential for use as a carrier for aerosolised salbutamol sulfate from dry powder inhalers. *European Journal of Pharmaceutical Sciences*, 19, 211–221.
- Lehr, C. M., Bouwstra, J. A., Schacht, E. H., & Junginger, H. E. (1992). In vitro evaluation of mucoadhesive properties of chitosan and some other natural polymers. *International Journal of Pharmaceutics*, 78, 43–48.
- Lim, D. S. T., Forbes, B., Martin, G. P., & Brown, M. B. (2001). In vivo and in vitro characterization of novel microparticulates based on hyaluronan and chitosan hydroglutamate. *AAPS PharmSciTech*, 2, 1–14.
- Lim, D. S. T., Forbes, B., Martin, G. P., & Brown, M. B. (2002). In vivo evaluation of novel hyaluronan/chitosan microparticulate delivery systems for the nasal delivery of gentamicin in rabbits. *International Journal of Pharmaceutics*, 231, 73–82.
- Mayol, L., Quaglia, F., Borzacchiello, A., Ambrosio, L., & La Rotonda, M. (2008). A novel poloxamers/hyaluronic acid in situ forming hydrogel for drug delivery: Rheological, mucoadhesive and in vitro release properties. *European Journal of Pharmaceutics and Biopharmaceutics*, 70, 199–206.
- Metz, G., Ziliox, M., & Smith, S. O. (1996). Towards quantitative CP-MAS NMR. *Solid State Nuclear Magnetic Resonance*, 7, 155–160.
- Mi, F.-L., Sung, H.-W., & Shyu, S.-S. (2000). Synthesis and characterization of a novel chitosan-based network prepared using naturally occurring cross linker. *Journal of Polymer Science: Part A: Polymer Chemistry*, 38, 2804–2814.
- Minne, A., Boireau, H., Horta, M. J., & Vanbever, R. (2008). Optimization of the aerosolization properties of an inhalation dry powder based on selection of excipients. *European Journal of Pharmaceutics and Biopharmaceutics*, 70, 839–844.
- Morales, M. E., Ruiz, M. A., Oliva, I., Oliva, M., & Gallardo, V. (2007). Chemical characterization with XPS of the surface of polymer microparticles loaded with morphine. *International Journal of Pharmaceutics*, 333, 162–166.
- Morimoto, M., Metsugi, K., Katsumata, H., Iwanaga, K., & Kakemi, M. (2001). Effects of low-viscosity sodium hyaluronate preparation on the pulmonary absorption of rh-insulin in rats. *Drug Development and Industrial Pharmacy*, 27, 365–371.
- Mustante, C. J., Schroeter, J. D., Rosati, J. A., Crowder, T. M., Hickey, A. J., & Martonen, T. B. (2002). Factors affecting the deposition of inhaled porous drug particles. *Journal of Pharmaceutical Sciences*, 91, 1590–1600.
- Muzzarelli, R. A. (1997). Human enzymatic activities related to the therapeutic administration of chitin derivatives. *Cellular and Molecular Life Sciences*, 53, 131–140.
- Oyarzun-Ampuero, F. A., Brea, J., Loza, M. I., Torres, D., & Alonso, M. J. (2009). Chitosan-hyaluronic acid nanoparticles loaded with heparin for the treatment of asthma. *International Journal of Pharmaceutics*, 381, 122–129.
- Pandey, R., & Khuller, G. K. (2005). Antitubercular inhaled therapy: Opportunities, progress and challenges. *Journal of Antimicrobial Chemotherapy*, 55, 430–435.
- Peer, D., & Margalit, R. (2004). Loading mitomycin c inside long circulating hyaluronan targeted nano-liposomes increases antitumor its activity in three mice tumor models. *International Journal of Cancer*, 108, 780–789.
- Rouse, J. J., Whateley, T. L., Thomas, M., & Eccleston, G. M. (2007). Controlled drug delivery to the lung: Influence of hyaluronic acid solution conformation on its adsorption to hydrophobic drug particles. *International Journal of Pharmaceutics*, 330, 175–182.
- Sahiner, N., & Jia, X. (2008). One-step synthesis of hyaluronic acid-based (sub)micron hydrogel particles: Process optimization and preliminary characterization. *Turkish Journal of Chemistry*, 32, 397–409.
- Saiò, H., Tuzi, S., & Naito, A. (1998). Polysaccharides and biological systems. In I. Ando, & T. Asakura (Eds.), *Solid State NMR of Polymers: Studies in physical and theoretical chemistry* (pp. 509–588). Elsevier Science.
- Schürch, S., Gehr, P., Im Hof, V., Geiser, M., & Green, F. (1990). Surfactant displaces particles toward the epithelium in airways and alveoli. *Respiratory Physiology*, 80, 17–32.
- Sham, J. O.-H., Zhang, Y., Finlay, W. H., Roa, W. H., & Löbnerberg, R. (2004). Formulation and characterization of spray dried powders containing nanoparticles for aerosol delivery to the lung. *International Journal of Pharmaceutics*, 269, 457–467.
- Sivadasa, N., O'Rourke, D., Tobin, A., Buckley, V., Ramtooil, Z., Kelly, J. G., et al. (2008). A comparative study of a range of polymeric microspheres as potential carriers for the inhalation of proteins. *International Journal of Pharmaceutics*, 358, 159–167.
- Stern, R., Kogan, G., Jedrzejak, M. J., & Šoltès, L. (2007). The many ways to cleave hyaluronan. *Biotechnology Advances*, 25, 537–557.
- Sung, J., Pulliam, B., & Edwards, D. (2007). Nanoparticles for drug delivery to the lungs. *Trends in Biotechnology*, 25, 563–570.
- Surendrakumarm, K., Martyn, G. P., Hodgson, E. C. M., Jansen, M., & Blair, J. A. (2003). Sustained release of insulin from sodium hyaluronate based dry powder formulations after pulmonary delivery to beagle dogs. *Journal of Controlled Release*, 91, 385–394.
- Taetz, S., Bocho, A., Surace, C., Arpicco, S., Renoir, J. M., Schaefer, U. F., et al. (2009). Hyaluronic acid-modified DOTAP/DOPE liposomes for the targeted delivery of anti-telomerase siRNA to CD44-expressing lung cancer cells. *Oligonucleotides*, 19, 103–116.
- Theocharis, D. A., Skandalis, S. S., Noulas, A. V., Papageorgakopoulou, N., Theocharis, A. D., & Karamanos, N. K. (2008). Hyaluronan and chondroitin sulfate proteoglycans in the supramolecular organization of the mammalian vitreous body. *Connective Tissue Research*, 49, 124–128.
- Vanbever, R., Mintzes, J. D., Wang, J., Nice, J., Chen, D., Batycky, R., et al. (1999). Formulation and physical characterization of large porous particles for inhalation. *Pharmaceutical Research*, 16, 1735–1742.
- Varshosaz, J. (2007). The promise of chitosan microspheres in drug delivery systems. *Drug Delivery*, 4, 263–273.
- Volpi, N., Schiller, J., Stern, R., & Soltès, L. (2009). Role, metabolism, chemical modifications and applications of hyaluronan. *Current Medicinal Chemistry*, 16, 1718–1745.
- Wang, J., Chua, K. M., & Wang, C. H. (2004). Stabilization and encapsulation of human immunoglobulin G into biodegradable microspheres. *Journal of Colloid and Interface Science*, 271, 92–101.
- Woo, J. S., Piao, M. G., Li, D. X., Ryu, D.-S., Choi, J. Y., Kim, J.-A., et al. (2007). Development of cyclosporin A-loaded hyaluronic microsphere with enhanced oral bioavailability. *International Journal of Pharmaceutics*, 345, 134–141.
- Xie, J., Marijnissen, J. C., & Wang, C. H. (2006). Microparticles developed by electro hydrodynamic atomization for the local delivery of anticancer drug to treat C6 glioma in vitro. *Biomaterials*, 27, 3321–3332.
- Xin, D., Wang, Y., & Xiang, J. (2010). The use of amino acid linkers in the conjugation of paclitaxel with hyaluronic acid as drug delivery system: Synthesis, self-assembled property, drug release, and In Vitro Efficiency. *Pharmaceutical Research*, 27, 380–389.
- Yang, W., Peters, J. I., & Williams, R. O., III. (2008). Inhaled nanoparticles – A current review. *International Journal of Pharmaceutics*, 356, 239–247.
- Zhuo, A., Guo, L., & Tang, L. (2003). Effect of an intrathoracic injection of sodium hyaluronic acid on the prevention of pleural thickening in excess fluid of tuberculous thoracic cavity. *Clinical and Experimental Pharmacology and Physiology*, 30, 203–205.